Correlation effects in transport properties of interacting nanostructures

A. Valli,[1] G. Sangiovanni,[1,2] A. Toschi,[1] and K. Held[1]

[1]*Institute of Solid State Physics, Vienna University of Technology, 1040 Vienna, Austria*

[2]*Institute for Theoretical Physics and Astrophysics, University of Würzburg, Am Hubland, D-97074 Würzburg, Germany*

(Received 2 May 2012; revised manuscript received 25 July 2012; published 14 September 2012)

We discuss how to apply many-body methods to correlated nanoscopic systems, and provide general criteria of validity for a treatment at the dynamical mean field theory (DMFT) approximation level, in which local correlations are taken into account, while nonlocal ones are neglected. In this respect, we consider one of the most difficult cases for DMFT, namely, for a quasi-one-dimensional molecule such as a benzene ring. The comparison against a numerically exact solution shows that nonlocal spatial correlations are relevant only in the limit of weak coupling between the molecule and the metallic leads and of low inter-atomic connectivity, otherwise DMFT provides a quantitative description of the system. As an application we investigate the role of correlations on electronic transport in quantum junctions, and we show that a local Mott-Hubbard crossover is a robust phenomenon in sharp nanoscopic contacts.

DOI: 10.1103/PhysRevB.86.115418 PACS number(s): 71.27.+a, 73.23.−b

I. INTRODUCTION

Strong electronic correlations are a big challenge in condensed matter theory. In the case of bulk materials, dynamical mean field theory (DMFT)[1] turned out to be a big breakthrough, at least in three dimensions. The reason for this is that local, time-dependent electronic correlations are taken into account accurately. This local part is the major contribution of electronic correlations at least for high enough coordination or dimensions or at elevated temperatures. For realistic materials calculations on the other hand, DMFT has been merged with density functional theory in the local density approximation (LDA).[2] All these calculations are done in the thermodynamic limit, i.e., for an infinitely extended crystal.

In nanoscopic systems, the confinement of electrons into low-dimensional structures is expected to enhance correlation effects compared to bulk materials. Since complex nanoscopic systems are nowadays experimentally available, a microscopic modeling of them together with a reliable solution method taking electronic correlations into account is highly desirable. In the context of transport through nanoscopic systems also the detailed modeling of the reservoirs is required to accurately describe the experimental data.

Very small nanoscopic systems and molecules consisting only of a few atoms can still be calculated exactly, i.e., the low-energy effective Hamiltonian for these can be solved, or for even simpler di- or tri-atomic molecules numerically exact solutions are possible, e.g., by quantum Monte Carlo (QMC)[3–5] or configuration interaction. However, as soon as the nanoscopic or molecular systems become somewhat more complex, this is not possible any longer and, hence, a reliable approximation is needed. Recently, there have been efforts to apply DMFT also to finite systems such as nanoscopic structures and molecules connected to reservoirs.[6,7] Since nanoscopic systems are very different from the bulk, at this early stage, we have first of all to learn how reliable DMFT for describing electronic correlations in nanoscopic and molecular systems is.

A general scheme for treating correlated nanoscopic systems should also include nonlocal spatial correlations beyond DMFT. In this respect, cluster[8] and diagrammatic extensions[9–13] have been developed. Among the diagrammatic extensions, the dynamical vertex approximation (DΓA)[9–12] represents a systematic improvement beyond DMFT, as it allows to calculate the nonlocal part of the self-energy under the assumption of locality for the two-particle fully irreducible vertex. Recently, it has been shown that the fully irreducible vertex is computationally accessible,[14] e.g., via the numerical solution of an Anderson impurity model (AIM). However, a full calculation for nanostructures at the DΓA approximation level, including the solution of the parquet equations,[9–12,16,17] is indeed computationally expensive.

In this paper we will focus on the DMFT approximation level, that can be seen as a special case of a general scheme that we call "nano-DΓA," as described in Ref. 6. In Sec. II, we outline the method and discuss the connection with related or alternative approaches. In Sec. III A, in order to understand the reliability of DMFT for nanoscopic systems, we compare it extensively to a numerically exact solution, in an interesting case of a quasi-one-dimensional molecule (benzene ring), and provide general criteria of validity for the approximation. In Sec. III B, we show the potentiality of the method applying it to single atom quantum junctions, namely, to quantum point contact (QPC) of different sizes. Finally, Sec. IV provides a summary and outlook.

II. METHOD

As pointed out in the introduction, we are interested in a nanoscopic system consisting of sites (e.g., atoms) i with an intersite hybridization (hopping) t_{ij}, a local Coulomb repulsion U_i and (optionally) a coupling $V_{i\nu k}$ to some noninteracting environment, describing metallic leads contacted to the nanostructure. The Hamiltonian hence reads

$$H = \sum_{ij\sigma} t_{ij} c^\dagger_{i\sigma} c_{j\sigma} + \sum_i U_i c^\dagger_{i\uparrow} c_{i\uparrow} c^\dagger_{i\downarrow} c_{i\downarrow} + \sum_{i\nu k\sigma} V_{i\nu k} c^\dagger_{i\sigma} l_{\nu k\sigma} + \text{H.c.} + \sum_{\nu k\sigma} \epsilon_{\nu k} l^\dagger_{\nu k\sigma} l_{\nu k\sigma}, \quad (1)$$

where $c^\dagger_{i\sigma}$ ($c_{i\sigma}$) and $l^\dagger_{\nu k\sigma}$ ($l_{\nu k\sigma}$) denote the creation (annihilation) operators for an electron with spin σ on site i and in lead ν

state k with energy $\epsilon_{\nu k}$. For the purposes of the present paper, the one-band Hamiltonian (1) is enough, because the main goal is to validate our approach. The extension to multiorbital problems is straightforward and below we will highlight the corresponding modifications to the general scheme.

Let us just recall here that a numerically exact solution of this problem suffers from a nonpolynomial growth of the computational effort with the system size and is hence limited by severe restrictions on the number of sites. Therefore, if one aims at dealing with complex structures made of more than a few coupled sites, some kind of approximation is needed. A DMFT-like approach with a suitable approximation may be able to deal with a large number of coupled correlated sites, but in order to apply DMFT—and its extensions—to nanoscopic systems, one needs to define a proper local impurity problem, whose solution (usually numerical) represents the bottleneck of the algorithm.

What one can do is to reduce the N-impurity Anderson problem (1) onto a set of independent auxiliary AIMs, one for each of the $N_{\rm ineq} \leqslant N$ inequivalent atoms in the nanostructure. Each AIM is a local problem that can be numerically solved to compute the $N_{\rm ineq}$ correspondent (local) self-energies, the knowledge of which allows to build a DMFT self-energy for the nanosctructure. The process is embedded into a self-consistency loop. This way the overall computational effort is heavily reduced, depending only linearly on $N_{\rm ineq}$, that in case of highly symmetric structures may be much lower than N. This procedure has, however, the drawback that nonlocal correlations within the nanostructure, which are expected to be relevant in low dimensions, are neglected. The treatment—when necessary—requires a more sophisticated analysis beyond the DMFT level.

The starting point of the method is the Green's function of the whole nanostructure (including the leads) $\hat{G}(z)$, which is a matrix in the site space, z being a (complex) variable indicating the (Matsubara) frequency. The generic matrix element of its inverse reads

$$\{\hat{G}^{-1}\}_{ij}(z) = z\delta_{ij} - t_{ij} - \sum_{\nu k} \frac{V_{i\nu k} V^*_{j\nu k}}{z - \epsilon_{\nu k}} - \Sigma_{ij}(z), \qquad (2)$$

where $\hat{\Sigma}(z)$ is the self-energy matrix describing the interaction between the impurity electrons. In the multiorbital case, the matrices $\hat{t}$, $\hat{V}$, $\hat{\Sigma}$, and $\hat{G}$ would also depend on orbital indices. All information about the geometry of the nanoscopic system is included in the hopping and in the hybridization matrices. At the model level, it is therefore straightforward to implement even extremely complex nanostructures. The input may come as well from an *ab intio* calculation, e.g., a local density approximation (LDA) projected to Wannier orbitals,[15] allowing for realistic calculations of nanoscopic systems and a quantitative comparison with experiments.

The general flowchart of the method is shown in Fig. 1 and is described below in more detail. (i) The first step consists of the definition of a local problem for each of the inequivalent atoms of the nanostructure, by means of the relation

$$\mathcal{G}^{-1}_{0i}(z) = [\{\hat{G}\}_{ii}(z)]^{-1} + \Sigma_{ii}(z). \qquad (3)$$

The dynamic Weiss field $\mathcal{G}_{0i}(z)$, $i = 1, \ldots, N_{\rm ineq}$, is built inverting the ith block of $\hat{G}$ and it contains the information

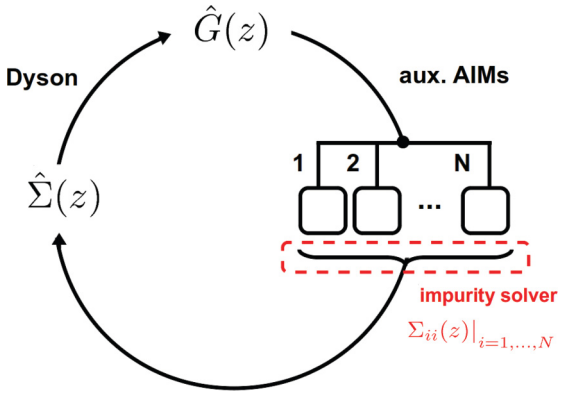

FIG. 1. (Color online) Flowchart of the DMFT self-consistency schemes for nanoscopic systems. The approximation consists in mapping the (nonlocal) problem of the whole nanostructure into a set of independent AIMs. The solution of these local problems yields a set of local self-energies, which can be used to define a DMFT self-energy for the nanostructure.

of the environment of site i, i.e., the rest of the nanostructure. In the multiorbital case, Eq. (3) becomes obviously a matrix equation with orbital indices. (ii) The numerical solution of each AIM yields a local (DMFT) self-energy $\Sigma_{ii}(z)$. All the $N_{\rm ineq}$ inequivalent self-energies are then collected and assigned to the corresponding equivalent sites as well, in order to build a self-energy matrix that is diagonal in the site index:

$$\hat{\Sigma}(z) = {\rm diag}[\Sigma_{11}(z), \Sigma_{22}(z), \ldots, \Sigma_{NN}(z)]. \qquad (4)$$

The self-energy $\hat{\Sigma}(z)$ is then plugged into Eq. (2) in order to compute the Green's function of the whole nanostructure and the process is iterated self-consistently till convergence.

The approximation involved in the present scheme is already known in the literature, and similar schemes have been applied to different kind of systems. An approach for quasi-one-dimensional systems is the chain DMFT by Biermann *et al.*,[18] where a system of weakly coupled (equivalent) chains is replaced by a single effective chain, coupled to a self-consistent bath. More, in general, the idea is suitable to the study of inhomogeneous systems and has been applied to, e.g., the study of bulk materials in the presence of two-dimensional interfaces by Potthoff and Nolting[19] as well as to the case of LDA + DMFT calculations with locally-inequivalent atoms within the unit cell (see, e.g., Ref. 20). Another noticeable case is its application to ultracold atoms on optical lattices, using the so-called real-space DMFT (R-DMFT), by Snoek *et al.*,[21] where the inhomogeneity comes from the external, spatially dependent, trapping potential, applied to an otherwise translationally invariant lattice. The present approach is similar to the R-DMFT, the difference being that in our case, each site is also coupled to a noninteracting bath, and a possible inhomogeneity arises not due to an external potential but from the geometry or even the chemical composition of the nanostructure itself.

The application of DMFT to nanoscopic systems, on the other hand, has been already attempted following alternative ways. A nano-DMFT scheme has been already proposed by Florens,[22] relying however on a specific cayley-tree geometry. Realistic calculations of strongly correlated transition metal

nanoscopic devices and of correlated adatoms on surfaces have been also recently carried out by Jacob *et al.*[23] and by Surer *et al.*,[24] respectively.

III. RESULTS

In the following, we will apply the presented DMFT method to various nanoscopic systems, in order to test the reliability of the approximation and to explore its potentialities. In this spirit, we extend the results presented in our previous work[6] computing several physical quantities, such as the occupations, local and nonlocal self energies, in the case of a benzene ring, where we can compare DMFT to a numerically exact solution. This allows us to show that our method is highly reliable in a wide range of parameters, but also to shed light on the physical role of the (missing) nonlocal correlations, which are responsible for the breakdown of the approximation.

Thereafter, the most natural step is to show the suitability of the method for more complex nanosystems. We focus our attention on quantum junctions in which electronic correlations are expected to be of importance due to both the confinement of electrons and the lack of a proper metallic screening at the atomic size contact. Even though in the literature many theoretical attempts to investigate transport at the mesoscopic scale can be found, the electron-electron interaction is usually either completely neglected or taken into account within possibly too simple approximation schemes.[25–28]

All the results presented below, for both DMFT and the exact solution, were obtained using Hirsch-Fye QMC[3] as an impurity solver for the AIM, unless otherwise stated. The use of a Hirsch-Fye algorithm limits us to high temperatures (about room temperature in the calculations presented here) but on the other hand it allows a quantitative comparison between the DMFT results and exact solution.

A. Benzene-like ring

A rather standard system in which the problem of understanding quantum transport phenomena is addressed is a benzene molecule, contacted with metallic (e.g., Au or Pt) electrodes. Therefore we study a nanostructure made of six correlated sites in the geometry of a benzene-like one-dimensional ring, given by Hamiltonian (1) with $i,j=1,\ldots,N=6$ and periodic boundary conditions. We consider here specifically a single orbital, which may not be a bad approximation for the benzene p_z orbital.[29] Our primary intention, however, is to systematically test our approximation for a simple model rather than a realistic calculation. Each site i has a hybridization channel $V_{i\nu k}$ to a metallic lead (labeled ν). In a typical experiment, two sites of the benzene molecule might be contacted by metallic wires. However, for the sake of simplicity and to deal with a system where all sites are fully equivalent, we consider each site to be contacted in an equivalent way to its own lead, i.e., $V_{i\nu k}=V\delta_{i\nu}$. The latter is not the only possibility to achieve the equivalence of all sites, but it represents a suitable configuration where one can study quantum electronic transport through a correlated nanostructure. A scheme of the nanostructure considered here is shown in Fig. 2.

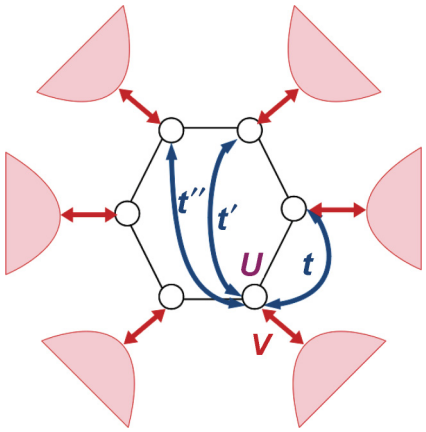

FIG. 2. (Color online) Scheme of the benzene ring. Empty circles represent correlated sites, with an on-site Hubbard repulsion U, connected between them via nearest neighbor (t) and longer range (t', t'') tunneling channels, and to metallic leads via hybridization channels (V).

In the calculations, two topologies of the hopping parameters are considered: (i) nearest-neighbor hopping t only (NN t) and (ii) for studying the effect of a higher connectivity (number of neighbors), equivalent hopping amplitude to all sites, i.e., nearest, next-nearest, and next-next-nearest neighbor hopping $t=t'=t''$ (all t). Of course, the latter is a rather unrealistic configuration since the hopping amplitude in a real molecule will decrease with distance, but it provides interesting insight into the validity of the approximation without introducing too many different hopping parameters.

We performed our DMFT calculations at fixed chemical potential, i.e., without considering the dependence on an applied gate voltage, assuming for the leads a flat density of states $\rho=1/2D$, where the half bandwidth $D=2t$. We compute site-dependent densities, double occupations, and the on-site spectral function

$$\overline{A(0)} = \int d\omega A(\omega)\cosh^{-1}(\omega/2T) = -\beta G(\beta/2), \qquad (5)$$

which can be extracted directly by the QMC.

In the inset of Fig. 3, we show noninteracting density of states $A^0(\omega)$ for the isolated molecule ($V/t=0$). In the NN t case, the benzene ring is half filled and insulating, the spectral function is symmetric with respect to the Fermi level, and the gap given by the bonding and antibonding combination of the kinetic term in the Hamiltonian. The all t case is also insulating but is not particle-hole symmetric. The results for $\overline{A(0)}$ as a function of the ratio between the hybridization strength V and the absolute value of the hopping amplitude t are shown in the main panel of Fig. 3. Looking at the NN t topology, we observe that the agreement between the exact solution and DMFT is very good when the hybridization V is large. In the limit $V\to\infty$, each atom forms a bound state with its own lead, hence the intersite (nonlocal) correlations become essentially negligible and DMFT works well. The opposite molecular limit $V/t\equiv 0.0$ is clearly the most difficult for DMFT. Indeed, the spectrum $\overline{A(0)}$ in Fig. 3 differs from the exact solution, which is gapped, while DMFT shows a small finite spectral weight.

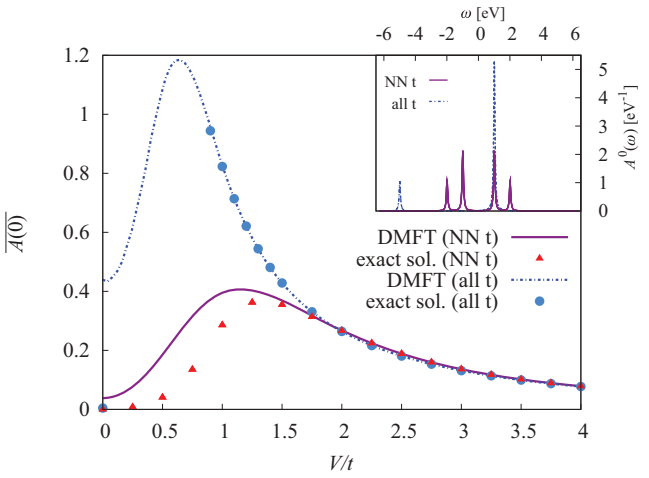

FIG. 3. (Color online) On-site spectral function $\overline{A(0)}$ as a function of V/t, comparing DMFT (lines) with the exact QMC solution (symbols) for both hopping to two nearest neighbors only (NN t) and to all neighbors (all t) configurations, at $U=5t$ and $T=0.05t$, taken from Ref. 6. Data for $V/t=0.0$ in the all t configuration are obtained by an exact diagonalization of the Hamiltonian. Inset: noninteracting density of states $A^0(\omega)=-(1/\pi)\mathrm{Im}G^0(\omega+\imath 0^+)$ for the isolated benzene molecule and both hopping configurations.

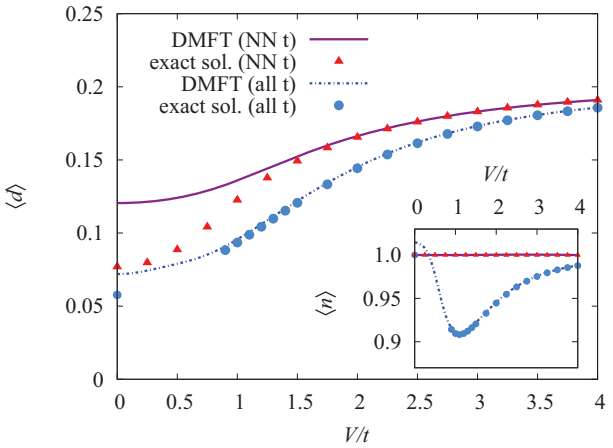

FIG. 4. (Color online) Double occupancies $\langle d\rangle=\langle n_\uparrow n_\downarrow\rangle$ as a function of V/t at $U=5t$ and $T=0.05t$, comparing DMFT (lines) and the exact solution QMC (symbols) for both hopping configurations. Data for $V/t=0.0$ in the all t configuration are obtained by an exact diagonalization of the Hamiltonian. Inset: corresponding densities $\langle n\rangle=\langle n_\uparrow+n_\downarrow\rangle$.

One expects that, upon increasing the connectivity, the DMFT description improves. In order to check this, we consider the all t topology as well. Indeed, we see in Fig. 3 that as the number of neighbors per atom is increased, no substantial difference to the exact solution can be found even in the intermediate region $V\sim t$ where deviations from the exact solution in the NN t case are already visible. Note that below $V=0.8t$, the exact QMC solution is not available any longer due to the fermionic sign problem, therefore, we cannot check the molecular limit for the all t topology at this value of U with such an impurity solver. The Hamiltonian of the isolated molecule can nevertheless still be diagonalized exactly also in the interacting case. The diagonalization predicts an insulating state also for the all t configuration, meaning that the approximation, even in the high connectivity case, will break down at low enough hybridization.

Similar agreement between DMFT and the exact solution is found for the site occupation, as shown in the inset of Fig. 4. In the NN t topology, the effect of the interaction and of the hybridization on the spectrum is to redistribute the spectral weight, with respect to the noninteracting case, in such a way that the system stays half filled. However, when the band structure is changed, and other hopping channels beyond the NN one are included, the density becomes t, U, and V dependent and the system may move away from half-filling. On the other side, concerning the double occupancy shown in the main panel, we can see that, for high connectivity and high values of V/t, corrections beyond DMFT are not important, while approaching the molecular limit the system is more spatially correlated than what DMFT suggests, overestimating double occupations.

A very clear explanation of the overall agreement shown above, between DMFT and the exact solution, is provided by the comparison of the respective self-energies for both hopping topologies, shown in Figs. 5 and 6. As usual, let us begin discussing the NN t case first, referring to Fig. 5, where we plot the corresponding self-energy in Matsubara representation. In Figs. 5(a)–5(c), the imaginary part of the local self-energy for different values of V/t is shown (the real part is zero due to the half-filling condition). One can see that the nanoapproximation nicely captures the local physics, accurately reproducing the exact self-energy at low frequencies, and thus providing a reliable estimate for the quasi-particle residue:

$$Z=\left(1-\left.\frac{\partial\mathrm{Im}\Sigma(\omega_n)}{\partial\omega_n}\right|_{\omega_n\to 0}\right)^{-1}. \tag{6}$$

Moreover, the amplitude of the local self-energy slightly decreases as V is increased, the system becoming less correlated and the agreement even improving.

However, the slope of the local self-energy at $\omega=0$ in some cases is clearly not enough to capture the full picture, and we have to take the nonlocal self-energy into account. This becomes evident analyzing the molecular limit $V/t=0$. In this limit and at finite U, the exact solution evidently predicts an insulating solution, as one can see from the absence of spectral weight at the Fermi level in the main panel of Fig. 3. The gap is controlled by U and is due to large nonlocal contributions of the self-energy, as shown in Figs. 5(d)–5(f). At the same time, in the noninteracting limit $U=0$, the isolated, half-filled, benzene molecule is a trivial band insulator. In this case, the Hamiltonian is made only of the kinetic term and the gap Δ is given by the energy difference between the bonding and antibonding eigenstates, $\Delta\sim 2t$. One can show, on the basis of simple arguments, that, in presence of nonlocal correlations, a suppression of the spectral weight at the chemical potential can be achieved by a large $\mathrm{Re}\Sigma_{i\neq j}$ even in the case of a linearly vanishing $\mathrm{Im}\Sigma_{ii}(\omega_n\to 0)$ as in Fig. 5(a).[30] Another interesting point concerning the results of Fig. 5 is that, upon increasing V, deviations from the exact results due to nonlocal correlations are quickly suppressed, while the local ones remain sizable. Approaching the limit $V\sim U$, of course, also local correlations are gradually suppressed.

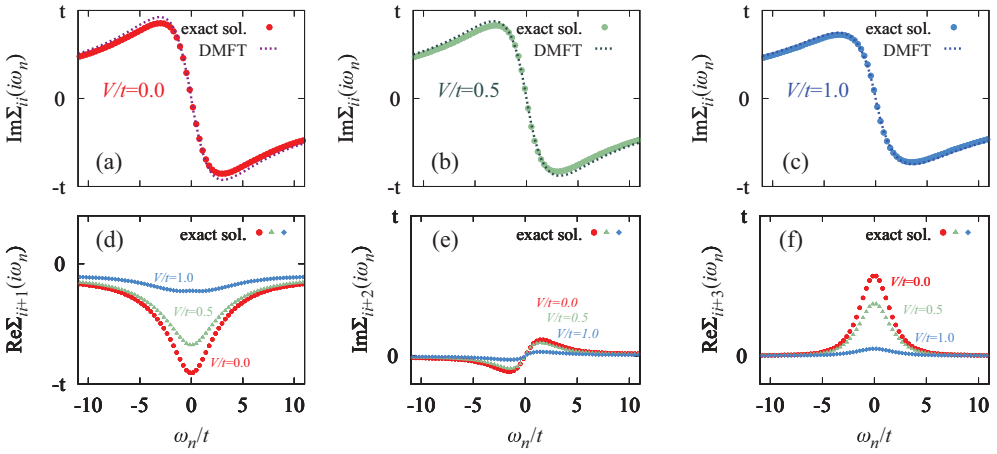

FIG. 5. (Color online) Self-energy in Matsubara representation for the benzene ring in the NN t topology at $U=5t$ and $T=0.05t$. In (a)–(c), we show the evolution with V/t of the imaginary part of the local self-energy, comparing DMFT (dashed lines) with the exact solution (symbols). Note that the real part is always identically zero due to the particle-hole symmetry at half-filling. In (d)–(f) we show the nonlocal self-energy of the exact solution for nearest-neighbors $(i, i+1)$, next-nearest neighbors $(i, i+2)$, and next-next-nearest neighbors $(i, i+3)$, respectively. All other nonlocal contributions are either identical to the ones shown here (since all sites are equivalent) or zero by symmetry. Note that $\Sigma_{i\neq j}$ is identically zero in DMFT.

These results can be summarized as follows. When the molecule is weakly connected to the contacts, one needs to go beyond DMFT, i.e., taking nonlocal correlations into account, in order to provide a good description of the system. On the other hand, in the region of intermediate hybridization coupling the most important role is played by the local physics, in a situation where the molecule is still strongly correlated. In many actual cases, this is the interesting region from the experimental point of view. This suggests that our method provides an accurate tool for describing the physics of correlated nanostructures, already at the DMFT approximation level. When nonlocal spatial correlations become non-negligible, one needs instead to go beyond DMFT.

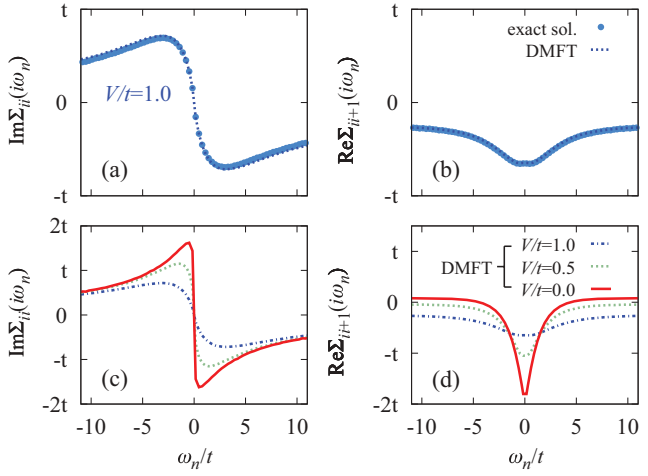

FIG. 6. (Color online) Local self-energy in Matsubara representation for the benzene ring in the all t topology at $U=5.0t$ and $T=0.05t$. Upper panels: comparison between DMFT (lines) and exact solution (symbols) at $V/t=1.0$. Nonlocal contributions to the self-energy are negligible with respect to the local ones (almost two orders of magnitude smaller) in contrast to the NN t case at the same value of V, and are therefore not shown. Lower panels: evolution of the DMFT self-energy, comparing the curves of the upper panel to the ones obtained for lower values of V/t, in a region where no exact QMC solution is available.

In addition to this, encouraging results come also from the analysis of the self-energy in the all t configuration, shown in Fig. 6. In Figs. 6(a) and 6(b), respectively, we show the comparison for the imaginary and the real part of the local self-energy at $V/t=1$, i.e., very close to the lowest value of V/t accessible to the QMC exact solution. The agreement between the curves is substantially perfect as expected on the basis of the previous analysis. Moreover, in this case, where the connectivity is higher with respect to the NN t hopping topology, any nonlocal contribution to the self-energy is already negligible with respect to the local ones, namely, almost two order of magnitude smaller (not shown). This means that the region where only the local physics is important extends to lower values of the hybridization when the connectivity is higher. Below this threshold, as discussed before, we can study the evolution of the self-energy toward the molecular limit only with DMFT. The results, in Figs. 6(c) and 6(d), show that the system is becoming more correlated upon decreasing V, i.e., the imaginary part of the local self-energy is increasing, and most likely also nonlocal correlations arise. Concerning the real part of the self-energy, it displays the formation of a peak-structure at low energy, while the large-frequency tail, determining the filling, tends toward zero as the system gets close to half-filling (compare also with the inset of Fig. 4).

In order to have a better picture of the behavior of the system, not limited to the Fermi level, we present in Fig. 7 the evolution with V/t, for both NN t and all t hopping configuration, of the spectral function $A(\omega)$, obtained via analytic continuation on the real axis of the DMFT(QMC) data using a Maximum Entropy method.[31] Already in the case of the isolated molecule, i.e., $V/t=0$, the spectral function of the interacting system shows substantial differences from the

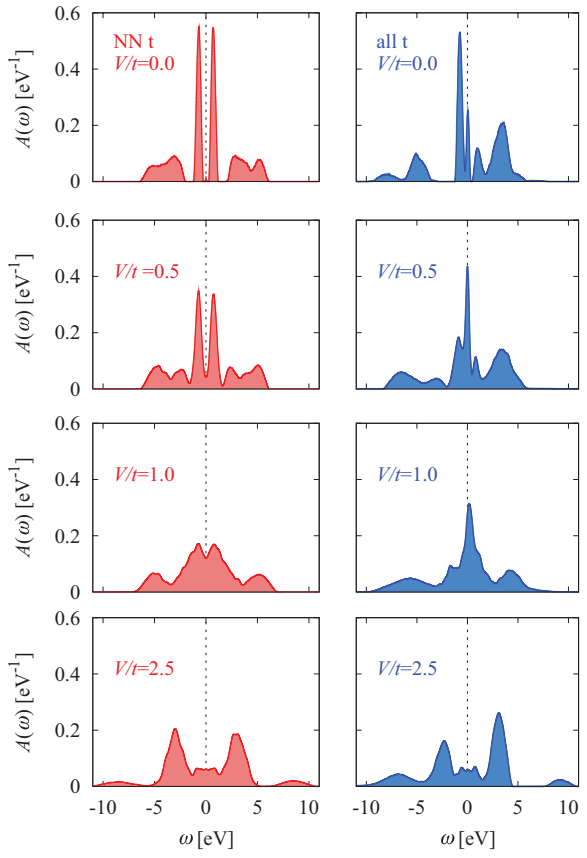

FIG. 7. (Color online) Evolution of the DMFT one-particle spectral function $A(\omega)$ with V/t, at $U=5t$ and $T=0.05t$, for both NN t and all t hopping configurations, according to the labels in the plots.

noninteracting one shown in the inset of Fig. 3. In the NN t topology, $A(\omega)$ retains two low energy peaks, symmetric with respect of the Fermi energy, corresponding to the bonding and antibonding peaks of the noninteracting spectrum, and some of the spectral weight is shifted to higher energies, forming a lower and an upper Hubbard band. Only some spectral weight fills the band gap, which is consistent with the previous finding of $\overline{A(0)}$ (main panel of Fig. 3) and with a linearly vanishing DMFT self-energy at $\omega = 0$, as shown in Fig. 5(a). The redistribution of the spectral weight due to the interaction is instead more drastic in the all t topology. The fivefold degenerate peak of the noninteracting spectrum disappears, as its degeneracy is lifted, and the resulting spectrum is metallic. This difference becomes even more important when the system is coupled to the leads. The hybridization to the metallic leads, on one hand, provides an additional broadening of the many-body states, via the so-called lead self-energy (or hybridization function), while on the other, it favors the emergence of a Kondo-like resonance at the Fermi energy in the single particle spectral function of each of the benzene sites. Therefore, in the all t topology, one can observe the formation of a narrow resonant peak at the Fermi energy in the spectral function, while in absence of electronic correlation the structure exhibits a fairly large gap at the Fermi level in both hopping configurations, and no resonant peak would exist. Upon increasing V, the resonance exhibits a maximum and is then suppressed. In the limit $V \gg t$, the hybridization becomes the dominating energy scale, the spectral weight is shifted to the Hubbard bands, and the spectral functions, in both hopping configurations, loose almost all low-energy features becoming similar to each other.

A very interesting issue deals with the study of electronic transport in correlated nanostructures. The conductance through the benzene ring $G(\omega)=(e^2/h)T(\omega)$ can indeed be computed along the lines of Refs. 32–36, using the Meir-Wingreen generalization of the Landauer formula. Here, e^2/h is the conductance quantum, e and h being the electron's charge and Planck's constant, respectively. The transmission function $T(\omega)$ is given by

$$T(\omega) = \mathrm{Tr}[\Gamma G^{\mathrm{r}}(\omega)\Gamma G^{\mathrm{a}}(\omega)], \tag{7}$$

where $G^{\mathrm{r,a}}$ are the retarded and the advanced Green's function, respectively, and the leads scattering amplitude is given by $\Gamma = 2\pi\rho V^2$. Note that Eq. (7) for the conductance neglects vertex corrections. It would nevertheless be exact if *all* sites of the benzene molecule are coupled symmetrically to the leads between which the conductance is computed.[34,35] However, in our case, Eq. (7) without vertex correction is an approximation. In the case of the benzene ring, if we restrict ourselves to the Fermi level, we can compute the transmission function between site i and j from the nonlocal interacting Green's function we obtain from the QMC as

$$T = T_{ij}(\omega = 0) = 2\Gamma_i |G_{ij}(\imath\omega_n \to 0)|^2 \Gamma_j, \tag{8}$$

where the factor 2 stems from spin degeneracy.

In the literature,[36] the conductance is usually calculated in the configuration where the molecule bridges two leads only. Depending whether the leads are connected to the nearest, next-nearest, or next-next-nearest (i.e., opposite) neighboring-sites of the benzene ring, those configurations are labeled as *ortho*-, *meta*-, and *para*-positions, respectively. For symmetry reasons, we have instead each site of the benzene ring equivalently coupled to its own lead. However, with this *caveat*, in the following, we keep the literature nomenclature and we refer to the transmission function of Eq. (8) in the channel $j=i+1$, $j=i+2$, and $j=i+3$, as the *ortho*-, *meta*-, and *para*-position transmission through the benzene ring, respectively, as shown in the upper panel of Fig. 8. The results for the zero-bias conductance as a function of the hybridization strength are shown in the lower panels of Fig. 8.

As a general remark, valid for all connections, we can see that G increases like V^4 at low values of the hybridization, as it could be expected from Eq. (8), treating the scattering amplitudes perturbatively. As V increases, G exhibits a maximum due to the formation of a Kondo resonance between each site and its own lead, which is then smeared out as $1/V^2$ as a consequence of the broadening of the resonance itself. In the all t topology, G is the same in all three contact positions, i.e., all positions are equivalent due to the particular hopping structure. The comparison between DMFT and the exact solution shows that nonlocal correlations are not important both in the limit in which the molecule is strongly coupled to the leads and when the connectivity is high, which, in the light of the results presented before, may not be surprising since

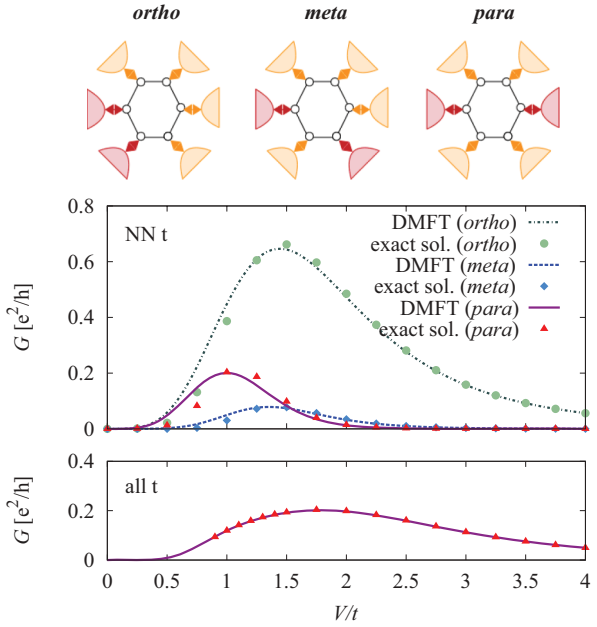

FIG. 8. (Color online) Conductance through the benzene ring as a function of the hybridization V to the leads, for NN t (upper panel) and all t (lower panel) hopping configurations at $U = 5t$ and $T = 0.05t$. In the all t case, due to the symmetry of the problem, all connections are equivalent. The *ortho*, *meta*, and *para* labels refer to the conductance computed between two of the metallic leads, as shown schematically above the plots.

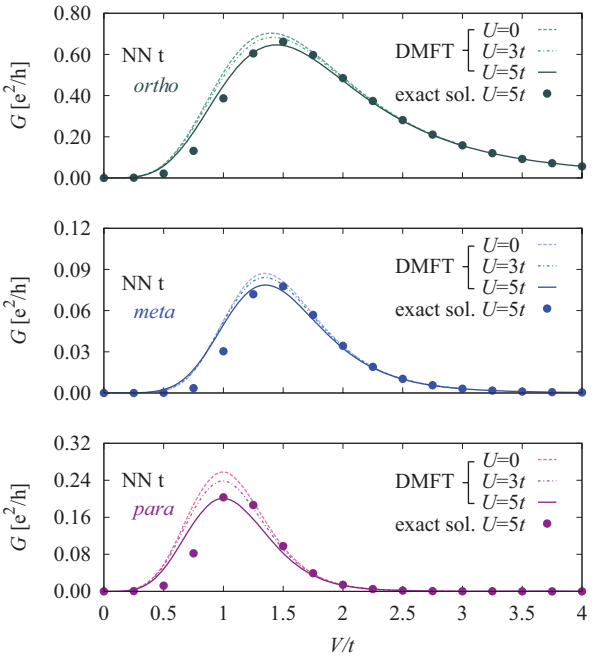

FIG. 9. (Color online) Conductance G in the three contact positions as a function of V/t for different values of U at $T = 0.05t$ in the NN t hopping configuration.

the conductance is computed out of the one-particle Green's functions, according to Eq. (8).

It is interesting to notice that, in the NN t topology, our calculation reproduces the reduction of the conductance in the *meta*-position, with respect to the *ortho*- and the *para*-position.[36] This effect is believed to be a generic characteristic of single molecule junctions, and it has been explained in terms of quantum interference in the transmission function, arising only from the molecule's topology and not directly related to the presence of electronic correlations.[37] On the other hand, many-body effects have been recently reported[38] to be responsible of the formation of transmission minima (so-called "Mott nodes") in molecules with open shell configurations. It is therefore interesting to analyze the influence of U on the profile of the zero-bias conductance. In Fig. 9, we report the results of our calculations at different values of U/t in the whole hybridization range. Note that in the noninteracting limit also DMFT is obviously exact. The main effect of U is to suppress the conductance peak, while the low- and high- hybridization regimes are not much affected. We compare the *percentage-wise* reduction $\Delta(U)$ of the conductance maximum at $U \neq 0$ with respect to its noninteracting value (at the same value of V) in order to get information on the effect of correlations *on top* of the topological reduction. We find out that the suppression increases with the distance between the sites through which the conductance is computed, i.e., $\Delta_{ortho} < \Delta_{meta} < \Delta_{para}$, as the Hubbard repulsion tends to localize the electrons in the molecule. We summarize the corresponding values in Table I.

B. Quantum junctions

In the current state-of-the-art of nanoscopic electronic transport, quantum junctions play a fundamental role. They can be experimentally realized by a mechanically controlled break (MCB) process of a metallic wire made, e.g., of Au, resulting in atomically sharp contacts with an adjustable tunneling gap. Strong evidences from conductance quantization have been reported, both at low[39] and at room temperature,[40] as a proof of the experimental realization of single atomic junctions. Moreover, molecules can be adsorbed into the gap, forming stable tunneling contacts, and allowing for the observation of electronic transport through molecular systems.[41]

One can expect electronic correlations to become relevant in the contact region, where electrons are spatially confined in narrow structures, as well as in the bridging molecule itself. In Ref. 6, we carried out a calculation on a model for a quantum junction made out of more than hundred correlated sites, showing that our method is able to handle even very complex nanostructures.

Before discussing the physical results we obtained, it is useful to recall the characteristic of the model junction. The system is made of two identical structures of correlated atoms with a simple body-centered cubic (bcc) lattice symmetry,

TABLE I. Percentage-wise reduction of the maximal conductance $\Delta(U)$ for *ortho*, *meta*, and *para* connections.

	$\Delta(U)$		
	ortho-	*meta*-	*para*-positions
$U = 5t$	∼7%	∼9%	∼22%
$U = 3t$	∼2%	∼3%	∼7%

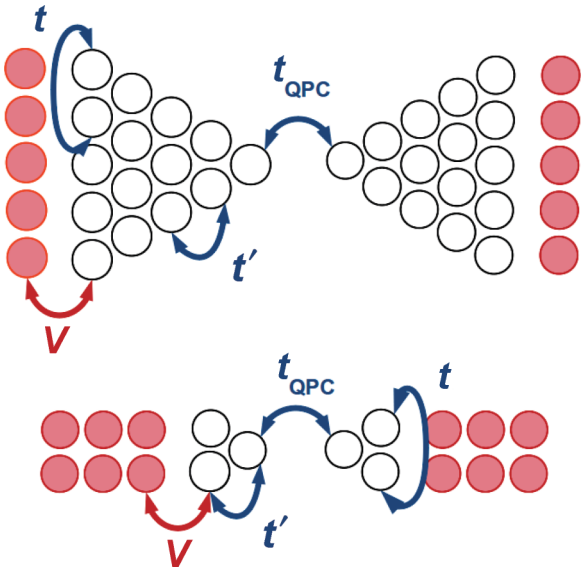

FIG. 10. (Color online) Scheme of the (three-dimensional) quantum junctions with five (upper panel) and two (lower panel) layers. Empty atoms have an on-site Hubbard repulsion U and are connected via hopping t, t', and hybridization V channels as schematically shown.

narrowed in a double-cone-like junction. For the sake of simplicity, we assume a single-band model, which may be suitable for cuprate or cobaltate junctions, though orbital selective tunneling processes will probably also play a role in, e.g., gold or aluminum devices. Hopping processes are allowed to nearest neighbor sites, both intralayer and interlayer, with amplitudes t and t', respectively, while the hopping between the tips is defined by the parameter $t_{\rm QPC}$. The outermost layer of each structure is connected via hybridization channels V to noninteracting leads, describing, e.g., the bulklike atoms of the wire. A scheme of junctions of different sizes we will discuss below is shown in Fig. 10.

In the previous paper,[6] we addressed the problem of what is happening at the junction in the MCB process, and we simulated the breaking of the junction by changing the distance $d_{\rm QPC}$ between the two structures thought the control parameter $t_{\rm QPC}$, i.e., the overlap of the electrons' atomic-like wave functions of the tip atoms. According to Ref. 42, $t_{\rm QPC}\sim(1/d_{\rm QPC}^{l+l'+1})\exp(-d_{\rm QPC})$, where l and l' are the angular momentum quantum numbers associated to the orbitals involved in the tunneling process. In the following, we calculate the distance d_{QPC} according to the above formula, where we suppose $l=l'=2$, i.e., a d-like orbital character for the correlated atom bands, however, the general physical argument discussed in the following does not depend on the precise dependence of $d_{\rm QPC}$ on $t_{\rm QCP}$.

We calculate the total transmission function through the junction summing over all possible transmission channels:

$$T=\sum_{ij}T_{ij}=2\frac{e^2}{h}\sum_{i\in L}\sum_{j\in R}\Gamma_i|G_{ij}(\imath\omega_n\to 0)|^2\Gamma_j, \qquad (9)$$

where L (left) and R (right) correspond to the correlated atoms sitting in the outermost layers of the junction. As $d_{\rm QPC}$ is increased DMFT reveals strong deviations from an exponential behavior of G, expected in the case of a tunneling process through a barrier. Such a result is associated to a local Mott-Hubbard crossover, occurring at the tip atom(s). It can be explained considering that the MCB process effectively removes a neighbor from the already poorly connected tip atoms. This further reduces the metallic screening of the local Coulomb interaction expected in the bulk, causing the tip to become more insulating-like. If correlations can so strongly influence the electronic structure of the contacts, this phenomenon could have a huge impact on the interpretation of experimental results, and it is therefore worth being investigated extensively.

The fundamental question to answer is whether the crossover is a generic characteristic of quantum junctions. Following Ref. 6, we performed calculations of the five-layer QPC (shown in the upper panel of Fig. 10) but for a slightly different set of parameters, more realistic for the bcc geometry considered here, where the intra- and interlayer hopping amplitudes t and t' are the same, and we choose $t=0.40$ eV. The results for such a structure are shown in Fig. 11. In the left panel, we show the conductance G through the five-layer QPC, as a function of $t_{\rm QPC}$, while we reproduce the same data as a function of the intertip distance $d_{\rm QPC}$ comparing to the noninteracting case on a logarithmic scale, so that the fingerprint of the Mott-Hubbard crossover, and its effect on electronic transport is highlighted: G shows a more-than-exponential suppression as a function of $d_{\rm QPC}$ for a value of $d_{\rm QPC}$ corresponding to $t_{\rm QPC}\sim t$, and recovers instead an exponential behavior at larger distances. In order to show that the relevant physics concerns the tip atoms, one can consider atom-resolved local quantities, i.e., the occupations and the local low-energy spectrum. We find that, due to the strong electronic correlations (provided that U/t is large enough, as it will be clarified in the following), the occupation $\langle n\rangle$ of all the atoms of the QPC stays at half-filling in the whole range of $t_{\rm QPC}$. Moreover, also the double occupations $\langle d\rangle$ and the low-energy spectrum $\overline{A(0)}$ of all layer atoms (i.e., all atoms except for the tip ones) are almost constant in the whole $t_{\rm QPC}$ range, their values naturally depending on the position of the atoms in the junction.

We find that a completely different behavior characterizes the tip atoms instead. In the right panels of Fig. 11, we restrict ourselves, for convenience, to the comparison of local quantities of just two representative atoms in the QPC, namely, the tip atom and one of the atoms sitting in the layer directly connected to the tip (denoted as layer atom in the following). Below $t_{\rm QPC}=0.60$ eV, both $\langle d\rangle$ and $\overline{A(0)}$ are continuously and monotonically suppressed as $t_{\rm QPC}$ decreases, confirming that the tip atoms undergo a local Mott crossover. One may further notice that the tips' $\overline{A(0)}$ reaches a maximum around $t_{\rm QPC}=0.60$ eV and decreases again for values of $t_{\rm QPC}$ above this threshold. This phenomenon is not correlation driven, as the double occupations always increase with increasing $t_{\rm QPC}$, but is caused by the recombination of the tip-atom states into a bonding and antibonding structure.

In order to better understand the physics behind this phenomenon, we significantly reduce the complexity of the problem. We consider a junction made of two layers (shown in the lower panel of Fig. 10) so that the tip atom is not connected directly to a bath of free electrons, but to a layer of correlated

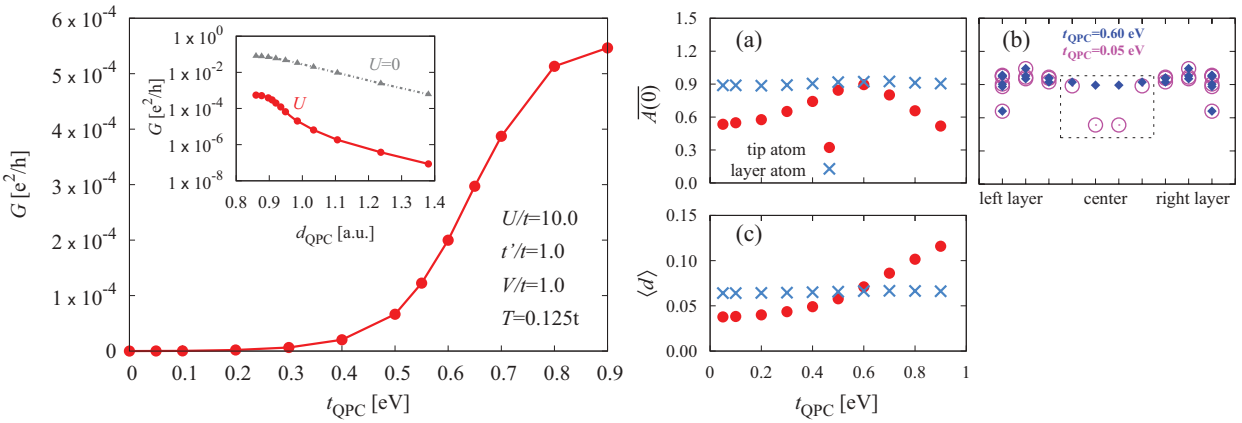

FIG. 11. (Color online) (Left) Conductance G through the five-layer QPC as a function of $t_{\rm QPC}$. The parameters are shown in the plot. (Inset) G as a function of an estimate of the intertip distance $d_{\rm QMC}$, as explained in the text. The data of the main panel (circles) are compared to the noninteracting case (triangles) on a logarithmic scale in order to highlight the effect of electronic correlations. (Right) Atom-resolved low-energy spectrum $\overline{A(0)}$ and double occupations $\langle d\rangle$. In (a) and (c), the dependence on $t_{\rm QPC}$ for the low-energy spectrum and the double occupations is shown for the tip-atom and an atom sitting in the layer closest to the tip. In (b), we show the low-energy spectrum for each inequivalent atom of the structure for two values of $t_{\rm QPC}$, namely, $t_{\rm QPC}=0.60$ eV (diamonds) and $t_{\rm QPC}=0.05$ eV (dotted circles). The change of $t_{\rm QPC}$ only affects the tip atoms. The region labeled with "center" and highlighted in the plot corresponds to the atoms analyzed in (a) and (c).

atoms. Therefore, there are by symmetry only two inequivalent atoms left, tip and layer atoms. This makes the system much simpler, but still allows us to observe a dichotomy between the two kinds of correlated atoms. Nevertheless it is important to stress that even this minimal model for the quantum junction cannot be solved exactly with QMC due to a severe fermionic sign problem.

From the evolution of the conductance through the junction for different values of U, it is clear that some critical value U^* exists above which G exhibits the more-than-exponential behavior associated with the Mott-Hubbard crossover, as shown in Fig. 12. The noninteracting QPC shows no peculiar feature, it evolves smoothly from the contact (small $d_{\rm QPC}$) to the tunneling (large $d_{\rm QPC}$) regime. As the value of U is increased, the conductance is globally suppressed, and above some threshold, it develops a much faster transition between the contact and tunneling regimes. In all cases, G does not reach the limit $G_0=e^2/h$ in the contact regime because of the absence of a completely open transmission channel. Similar observation on MCB junctions[43] or on the tunneling spectra of Co impurities adsorbed on a Cu(100) surface[44] supports the hypothesis that such effects, which we show to be

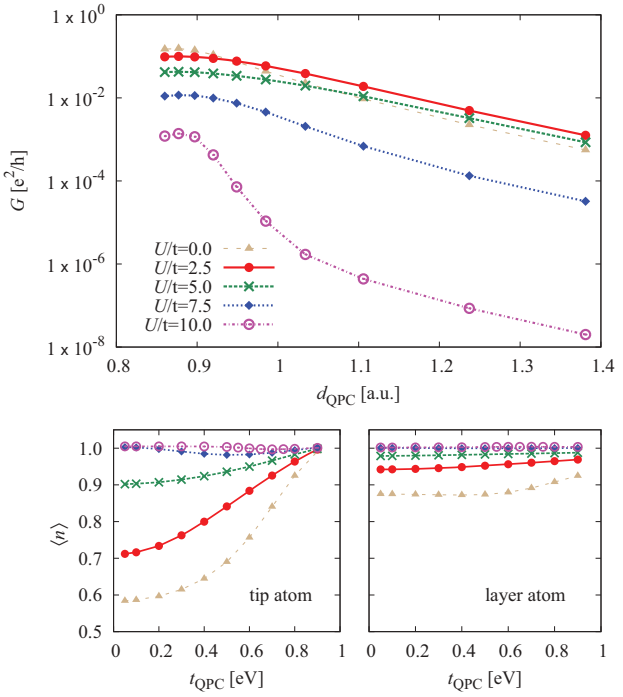

FIG. 12. (Color online) (Top) Conductance G through the two-layer QPC vs $d_{\rm QPC}$ for different values of U/t. (Bottom) Corresponding density of the two inequivalent atoms according to the labels in the plot.

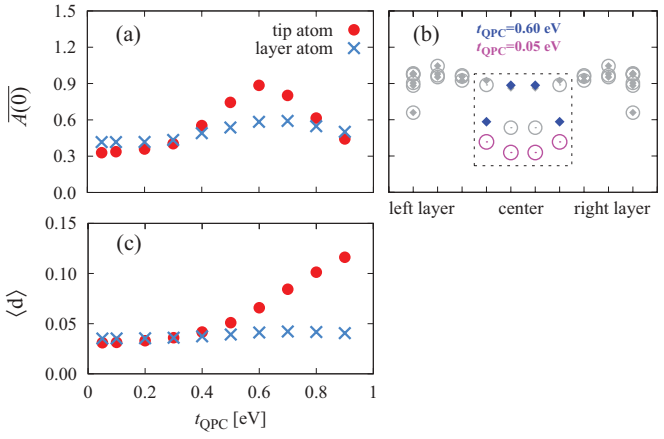

FIG. 13. (Color online) (Left) Atom-resolved double occupations $\langle d\rangle$ and low-energy spectrum $\overline{A(0)}$ as a function of $t_{\rm QPC}$ at $U=10t>U^*$ and $T=0.125t$. (Right) $\overline{A(0)}$ for each of the structure inequivalent atoms for two values of $t_{\rm QPC}$, namely, $t_{\rm QPC}=0.60$ eV (diamonds) and $t_{\rm QPC}=0.05$ eV (dotted circles). The region labeled with "center" and highlighted in the plot corresponds to the atoms analyzed in (a) and (c). Light shaded data are the corresponding values of the spectrum of the five-layer QPC, for comparison.

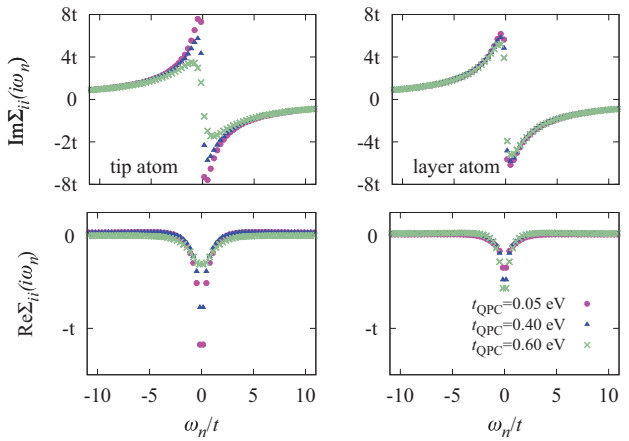

FIG. 14. (Color online) Layer-resolved DMFT local self-energy in Matsubara representation of the only two inequivalent atoms (i.e., tip atom and layer atom, according to the labels in the plot) of the two-layer QPC for $U = 10t > U^*$ and $T = 0.125t$ for different values of t_{QPC}. While the tip atom is strongly affected by t_{QPC}, the layer atom exhibits no significant dependence.

driven by correlations, can be of importance in experiments. In order to relate the behavior of G with a Mott-Hubbard transition, we also look at the layer-resolved $\overline{A(0)}$, in analogy to the five-layer QPC. One has anyway to be careful here, because below a critical U, the spectral weight is affected by strong t_{QPC}-dependent density fluctuations. On the other hand, approaching U^* all atoms occupations tend toward half-filling (see Fig. 12 lower panels) and the analysis of the spectral weight for this purpose is safe.

In Fig. 13, we show the results for the low-energy spectrum $\overline{A(0)}$ and the double occupations $\langle d \rangle$ at a value of U above the critical one ($U > U^*$), analogously to the case of the five-layer QPC. We can observe that below the threshold value $t_{QCP} = 0.60$ eV both $\langle d \rangle$ and $\overline{A(0)}$ for the tip atoms decrease continuously with t_{QPC} as the tip atom becomes more insulating-like. The overall behavior for the tip atom of the different size QPCs is qualitatively very similar, suggesting the existence of a (size-independent) energy scale associated with this phenomenon. One can notice that in the two-layer QPC the layer atoms' local quantities show some dependence on t_{QPC}, and the values of the double occupations and of the low-energy spectrum of the layer atoms are slightly reduced compared to the corresponding one of the five-layer QPC. This indicates correlation effects to be further enhanced upon decreasing the system size.

One can indeed check that, considering junctions of intermediate size with respect to the ones shown here, i.e., adding one layer after the other to the two-layer QPC, helps the stabilization of both the local quantities of the layer atoms, which loose almost any dependence on t_{QPC}, while the tip atoms still display a local Mott-Hubbard transition.

Another clear evidence of the enhancement of electronic correlations in the MCB process is also provided by the evolution with t_{QPC} of the DMFT self-energy. In Fig. 14, we show the imaginary and real part of the local self-energy for both inequivalent atoms of the two-layer QPC at $U = 10t$ ($U > U^*$). As already mentioned, the MCB process confines the tip atom(s) at the edge of the structure, and drastically suppressing the hopping channel in one direction further reduces the screening of the Coulomb repulsion. Consequently, electronic correlations in the tip atom are strongly enhanced determining a local Mott-Hubbard crossover in the tip, while the layer-atom self-energy does not show significant dependence on t_{QPC}. Below the critical U instead, one finds a dependence on t_{QPC} only in $\mathrm{Re}\Sigma_{ii}(\imath\omega)$, i.e., in the renormalization of the chemical potential, responsible for the change in the occupancy (not shown). The above analysis shows once more that the change in the conductance in the MCB process can be traced back to the strong electronic correlations arising from the spatial confinement of electrons in sharp contact devices.

IV. CONCLUSIONS AND OUTLOOK

We have studied electronic correlations in nanoscopic systems within a many-body approach suitable to deal with complex correlated structures. We show that including local electronic correlations we can reasonably describe nanoscopic systems with many neighbors, long-range hopping, or a sufficiently strong hybridization to noninteracting leads. These conditions are fulfilled in many cases of interest, but there are regimes in which nonlocal self-energies are observed and it becomes necessary to also include spatial correlations beyond DMFT. We therefore plan to generalize the present method within the framework of DΓA, in order to include spatial correlations at all length scales. This way we expect to be able to recover a reliable description of the nanoscopic system on an even larger parameter range. The present approach can be viewed as the $n = 1$ particle level of a more general nanoscopic DΓA scheme. It could be an important tool for investigating electronic transport in correlated structures at the nanoscale. In this respect, we also studied, as a potential application, the transport through a MCB junction. Going beyond Ref. 6, we investigated the phenomenon of a local Mott-Hubbard crossover in quantum junctions of different sizes, showing that it is a general feature of sharp nanostructures and that it may be of importance for the interpretation of experiments.

ACKNOWLEDGMENTS

We would like to thank in particular Olle Gunnarsson who strongly contributed to the early stages of this study and S. Andergassen for suggestions and a very careful reading of the manuscript. Discussions with M. Capone, C. Castellani, S. Ciuchi, C. Di Castro, J. Lorenzana, G. Rohringer, and D. Rotter are also acknowledged. We acknowledge financial support from the Austrian Science Fund (FWF) through F4103-N13 (AV), I610-N16 (AT), and I597-N16 (KH). Calculations have been performed on the Vienna Scientific Cluster.

[1]W. Metzner and D. Vollhardt, Phys. Rev. Lett. **62**, 324 (1989); A. Georges and G. Kotliar, Phys. Rev. B **45**, 6479 (1992); A. Georges, G. Kotliar, W. Krauth, and M. Rozenberg, Rev. Mod. Phys. **68**, 13 (1996).

[2]V. I. Anisimov, A. I. Poteryaev, M. A. Korotin, A. O. Anokhin, and G. Kotliar, J. Phys.: Cond. Matter **9**, 7359 (1997); A. I. Lichtenstein and M. I. Katsnelson, Phys. Rev. B **57**, 6884 (1998); K. Held, I. A. Nekrasov, G. Keller, V. Eyert, N. Blümer, A. McMahan, R. Scalettar, T. Pruschke, V. I. Anisimov, and D. Vollhardt, Phys. Status Solidi B **243**, 2599 (2006); G. Kotliar, S. Y. Savrasov, K. Haule, V. S. Oudovenko, O. Parcollet, and C. A. Marianetti, Rev. Mod. Phys. **78**, 865 (2006); K. Held, Adv. Phys. **56**, 829 (2007).

[3]J. E. Hirsch and R. M. Fye, Phys. Rev. Lett. **56**, 2521 (1986).

[4]T. Maier, M. Jarrell, T. Pruschke, and M. H. Hettler, Rev. Mod. Phys. **77**, 1027 (2005).

[5]E. Gull, A. J. Millis, A. I. Lichtenstein, A. N. Rubtsov, M. Troyer, and P. Werner, Rev. Mod. Phys. **83**, 349 (2011).

[6]A. Valli, G. Sangiovanni, O. Gunnarsson, A. Toschi, and K. Held, Phys. Rev. Lett. **104**, 246402 (2010).

[7]N. Lin, C. A. Marianetti, A. J. Millis, and D. R. Reichman, Phys. Rev. Lett. **106**, 096402 (2011).

[8]M. H. Hettler, A. N. Tahvildar-Zadeh, and M. Jarrell, Phys. Rev. B **58**, R7475 (1998); A. I. Lichtenstein and M. I. Katsnelson, *ibid*. **62**, R9283 (2000); G. Kotliar, S. Y. Savrasov, G. Pálsson, and G. Biroli, Phys. Rev. Lett. **87**, 186401 (2001); M. Potthoff, M. Aichhorn, and C. Dahnken, *ibid*. **91**, 206402 (2003); T. Maier, M. Jarrell, T. Pruschke, and M. Hettler, Rev. Mod. Phys. **77**, 1027 (2005).

[9]A. Toschi, A. A. Katanin, and K. Held, Phys. Rev. B **75**, 045118 (2007).

[10]K. Held, A. A. Katanin, and A. Toschi, Prog. Theor. Phys. Suppl. **176**, 117 (2008).

[11]A. A. Katanin, A. Toschi, and K. Held, Phys. Rev. B **80**, 075104 (2009).

[12]A. Toschi, G. Rohringer, A. A. Katanin, and K. Held, Ann. Phys. **523**, 698 (2011).

[13]C. Slezak, M. Jarrell, T. Maier, and J. Deisz, J. Phys.: Condens. Matter **21**, 435604 (2009); A. N. Rubtsov, M. I. Katsnelson, and A. I. Lichtenstein, Phys. Rev. B **77**, 033101 (2008); also see H. Kusunose, J. Phys. Soc. Jpn. **75**, 054713 (2006).

[14]G. Rohringer, A. Valli, and A. Toschi, Phys. Rev. B **86**, 125114 (2012).

[15]J. Kunes, R. Arita, P. Wissgott, A. Toschi, H. Ikeda, and K. Held, Comp. Phys. Commun. **181**, 1888 (2010).

[16]N. E. Bickers, *Self-consistent many-body theory for condensed matter systems* (Addison Wesley, New York, 1998).

[17]S. X. Yang, H. Fotso, J. Liu, T. A. Maier, K. Tomko, E. F. D'Azevedo, R. T. Scalettar, T. Pruschke, and M. Jarrell, Phys. Rev. E **80**, 046706 (2009); Ka-Ming Tam, H. Fotso, S.-X. Yang, Tae-Woo Lee, J. Moreno, J. Ramanujam, and M. Jarrell, arXiv:cond-mat/1108.4926v2.

[18]S. Biermann, A. Georges, A. Lichtenstein, and T. Giamarchi, Phys. Rev. Lett. **87**, 276405 (2001).

[19]M. Potthoff and W. Nolting, Phys. Rev. B **60**, 7834 (1999).

[20]H. Das, G. Sangiovanni, A. Valli, K. Held, and T. Saha-Dasgupta, Phys. Rev. Lett. **107**, 197202 (2011).

[21]M. Snoek, I. Titvinidze, C. Tőke, K. Byczuk, and W. Hofstetter, New J. Phys. **10**, 093008 (2008).

[22]S. Florens, Phys. Rev. Lett. **99**, 046402 (2007).

[23]D. Jacob, K. Haule, and G. Kotliar, Phys. Rev. Lett. **103**, 016803 (2009); Phys. Rev. B **82**, 195115 (2010).

[24]B. Surer, M. Troyer, P. Werner, T. O. Wehling, A. M. Läuchli, A. Wilhelm, and A. I. Lichtenstein, Phys Rev. B **85**, 085114 (2012).

[25]M. Wierzbowska, A. Delin, and E. Tosatti, Phys. Rev. B **72**, 035439 (2005).

[26]J. C. Cuevas, A. Levy Yeyati, and A. Martin-Rodero, Phys. Rev. Lett. **80**, 1066 (1998).

[27]E. Scheer, N. Agraït, J. C. Cuevas, A. Levy Yeyati, G. Ludoph, A. Martin-Rodero, G. R. Bollinger, J. M. van Rultenbeek, and C. Urbina, Nature (London) **394**, 154 (1998).

[28]M. Häfner, J. K. Viljas, D. Frustaglia, F. Pauly, M. Dreher, P. Nielaba, and J. C. Cuevas, Phys. Rev. B **77**, 104409 (2008).

[29]A realistic calculation of Benzene might also require to include nonlocal Coulomb interactions.[7] This is only possible in a suggested extension of DΓA.[12]

[30]A. Valli, G. Rohringer, A. Toschi, G. Sangiovanni, and K. Held (unpublished).

[31]J. E. Gubernatis, M. Jarrell, R. N. Silver, and D. S. Sivia, Phys. Rev. B **44**, 6011 (1991).

[32]R. Landauer, IBM J. Res. Dev. **1**, 223 (1957).

[33]M. Büttiker, Phys. Rev. Lett. **57**, 1761 (1986).

[34]Y. Meir and N. S. Wingreen, Phys. Rev. Lett. **68**, 2512 (1992).

[35]A. Georges and Y. Meir, Phys. Rev. Lett. **82**, 3508 (1999).

[36]G. C. Solomon, D. Q. Andrews, T. Hansen, R. H. Goldsmith, M. R. Wasielewski, R. P. Van Duyne, and M. R. Ratner, J. Chem. Phys. **129**, 541701 (2008).

[37]T. Markussen, R. Stadler, and K. S. Thygesen, Nano Lett. **10**, 4260 (2010).

[38]J. P. Bergfield, G. C. Solomon, C. A. Stafford, and M. A. Ratner, Nano Lett. **11**, 2759 (2011).

[39]B. J. van Wees, H. van Houten, C. W. J. Beenakker, J. G. Williamson, L. P. Kouwenhoven, D. van der Marel, and C. T. Foxon, Phys. Rev. Lett. **60**, 848 (1988).

[40]C. J. Muller, J. M. Krans, T. N. Todorov, and M. A. Reed, Phys. Rev. B **53**, 1022 (1996).

[41]A. Reed, C. Zhou, C. J. Muller, T. P. Burgin, and J. M. Tour, Science **278**, 252 (1997).

[42]J. M. Blanco, F. Flores, and R. Perez, Prog Surf. Sci. **81**, 403 (2006).

[43]J. M. Krans, C. J. Muller, I. K. Yanson, T. C. M. Govaert, R. Hesper, and J. M. an Ruiteneek, Phys. Rev. B **48**, 14721 (1993).

[44]N. Néel, J. Kröger, L. Limot, K. Palotás, W. A. Hofer, and R. Berndt, Phys. Rev. Lett. **98**, 016801 (2007).